ORIGINAL PAPER

Akshay Prakash Kalgutkar · Sauvik Banerjee

Buckling behaviour of the stiffened hygrothermally stable composite plates with interfacial debond subjected to environmental and operational loading conditions

Abstract Due to the advantage of strength enhancement without increasing the structural weight, stiffeners are commonly used in many engineering structures. However, during their service life, these stiffened structures are usually exposed to an extreme environment, which may cause damage. Most of the researchers have carried out the work to study the unreinforced plate's stability behaviour considering interlaminar skin debonding in the hygrothermal condition. However, in the current investigation, the buckling capacity of stiffened composite plates debonded at the contact of plate and stiffener under non-uniform edge loading in hygrothermal conditions is studied. The study is performed by developing a computationally efficient finite element formulation. In the present research, the plate and the flange of T-stiffener are formulated by adopting a 9-noded heterosis element preventing the shear locking. In contrast, a 3-noded isoparametric beam element is used to formulate the stiffener web by accommodating the torsion correction factor, considerably reducing the computational cost. In the current study, the debond is modelled by creating a dummy node, and further interpenetration of the nodes is prevented by introducing a fictitious spring in the debonded region. Due to the highly uneven stress variation, a dynamic approach is employed to estimate the buckling constant by utilizing two sets of boundary conditions. Three schemes of hygrothermally stable laminates $(\theta/(90-\theta))_s$, $(22.5/-67.5)_s$, and $(77.5/-12.5)_s$ are considered to identify the stiffened plate configuration with enhanced buckling capacity when subjected to various non-uniform loading patterns. Further, extensive parametric investigations are conducted on the obtained stiffened plate with improved performance under a hygrothermal environment by considering debond at the skin–stiffener interface. It is found that debonded plate's stability is substantially affected by moisture. On the other hand, depending on the stiffener position and hygrothermal load intensity, the stiffener's depth-to-width ratio substantially affects the debonded plate's stability. Therefore, this investigation can be considered as a benchmark study for the stability performance of the debonded reinforced composite panel, which partially reduces the 2-D problem to 1-D element, thereby improving the computational cost.

1 Introduction

The majority of the engineering structures are usually supported on the stiffener, as they provide better resistance to buckling modes without significantly increasing the overall structural weight. However, these are subjected to multi-field loading in highly complex operating environments. Also, the manifestation of thermal stresses and moisture absorption significantly impact the composite structure's performance, which will degrade the elastic modulus at a higher temperature intensity or moisture concentration that might damage the structure. The presence of delamination or any other discontinuities in composite laminates detrimentally affects the

A. P. Kalgutkar · S. Banerjee (✉)
Department of Civil Engineering, Indian Institute of Technology Bombay, Mumbai 400 076, India
e-mail: sauvik@civil.iitb.ac.in

A. P. Kalgutkar
e-mail: akshay_kalgutkar@iitb.ac.in

structure's safety and durability. Hence, it becomes considerably important to have extensive knowledge of the buckling characteristics of the debonded stiffened composite plate exerted with a non-uniform edge load exposed to hygrothermal environment, which has received considerable attention recently.

Analysing composite structures is extremely difficult because of the coupling between torsion, membrane, and bending strains, and mechanical characteristics discontinuity across the laminate thickness. Due to this, displacement-based theories are widely used in the analysis of laminated as well as sandwich structures. Among the various theories, 3D continuum-based theories can more accurately determine the response of laminates but involves high computational cost. However, the equivalent single-layer (ESL) model reduces the considered problem to a 2D problem by expressing the displacement field as the mid-plane variable, significantly reducing the computational cost. The use of analytical/ numerical techniques in accordance with various 2D and 3D theories has piqued the research group's interest. A detailed review of the different computational methods used for the hygrothermal analysis is provided by Garg et al. [1].

Many researchers [2–5] have been inspired to examine the stability behaviour of plates applied to uniform edge loads in recent years. The static and stability characteristics of plates, beams, and shells were studied by Kumar [6] by briefly reviewing the Rayleigh–Ritz method employing various theories. Plates are usually found as components of larger structures. So, this minor portion may not be evenly under load due to its interaction with the adjoining part. Therefore, a non-uniform load distribution must be considered for a realistic investigation of the components. Few researchers [7–13] have investigated static stability performance of unreinforced and reinforced plates with beam stiffener under non-uniform edge loads by employing the first and higher-order theories. Numerous investigations are available that considered the buckling capacity of the delaminated plate. Many researchers [14–16] have investigated the stability behaviour of plates by considering the delamination of different shapes along the laminate thickness using the finite element method (FEM). They divided the debonded zone into sublaminates and employed displacement continuity conditions at the edges. Further, Yap et al. [17] performed a buckling and post-buckling investigation of a T-stiffened plate debonded at the interface of plate and stiffener by employing MSC Nastran. However, they used plate elements to model the stiffener. On the contrary, Ovesy et al. [18] studied the debonded plate's stability and vibration behaviour using two variations of the finite strip method (FSM) approaches, semi-analytical and spline methods.

Later, the thermal stability characteristics of the clamped rectangular plate were investigated analytically by Al-Khaleefi et al. [19] using first-order shear deformation theory. Further, Cui et al. [20] conducted a study investigating the thermal stability and the dynamic behaviour of a simply supported plate with adjacent in-plane stick-slipstop boundaries. Their main motto was to investigate the effects of normal forces and clearances on the thermal stability and vibration behaviour of the plate under temperature. On the other hand, a handful of researchers investigated the stability behaviour of skin-delaminated plates under hygrothermal loading. Panda et al. [21] experimentally and numerically examined the stability performance of interlaminar debonded plates under hygrothermal conditions. Further, by using the third-order shear deformation theory (TSDT), Nikrad et al. [22] inspected the thermal instability behaviour of delaminated composite plates by considering the von Karman geometric nonlinearity. The thermal buckling and post-buckling characteristics of the rectangular composite plate under localized heating was studied by Kumar et al. [23] by using the semi-analytical method. Later on, vibration and buckling characteristics of the delaminated plate were investigated by Amoushahi et al. [24] by using FSM. They have employed temperature-dependent material properties for the analysis. On the other hand, Mondal et al. [25] used the layerwise B-spline finite element method to investigate the thermal stability of the delaminated plate exposed to localized heating. They employed a step function in the delamination zone to represent jump discontinuities. Recently, Xia et al. [26] examined the buckling and post-buckling capacity of the debonded Reissner–Mindlin composite plates by using an obtained asymptotic solution for the delaminated composite plate.

The review shows that extensive investigation has been conducted on the buckling behaviour of delaminated composite plates and beams over the last two decades from both linear and nonlinear perspectives. Also, a significant amount of work is available on the stability characteristics of the laminated plate under the effect of hygrothermal loading. However, a handful of research has been conducted to study the buckling strength of the skin-delaminated plate under exposure to hygrothermal conditions. To the best of author's knowledge, no research was carried out that deals with the buckling capacity of debonded stiffened plates under hygrothermal conditions. Furthermore, using an appropriate theory to examine the impact of environmental loading on plate behaviour is critical. Material properties variation, as well as structural expansion, is observed with the exposure to hygrothermal load. As the loading intensity varies along the thickness, it becomes critical to employ an appropriate model to predict the thermal, hygral, and thermomechanical properties. Chamis et al. [27], Noor et al. [28], and Garg et al. [1] explained the various approaches to predict these properties.

In the current investigation, the authors have attempted to examine the debonded stiffened composite plate's buckling capacity under non-uniform edge load exposed to hygrothermal condition by employing the FE approach. For this, a reliable FE code is developed in MATLAB. In the earlier studies, the entire stiffened plate was formulated by employing a 3-D brick element or a 2-D shell element, which were computationally expensive. However, in the present work, the plate and the flange of the stiffener are represented by employing a 9-noded heterosis element, preventing the shear locking. In contrast, the stiffener web uses a 3-noded isoparametric beam element that incorporates the torsion correction factor, reducing the computational cost. The debond is modelled by splitting the parent nodes into independent dummy nodes and inserting a fictitious spring to avoid interpenetration of nodes. In the bonded region, the displacement continuity condition is employed at the interface of the plate and flange to emphasize the nodal displacement of the flange in terms of the plate's nodal displacement. The study takes into account a uniform distribution of hygrothermal load across the thickness, and hygrothermal load-dependent material properties are used in the analysis. The investigation considers three hygrothermally stable plates with lamina schemes of $(\theta/90-\theta)_s$, $(22.5/-67.5)_s$ and $(77.5/-12.5)_s$ that are subjected to six different non-uniform loading patterns. Initially, an investigation is carried out to ascertain a suitable lamina scheme and loading pattern based on the improved buckling strength of the plate. Further, extensive parametric studies are conducted on the determined stiffened plate with enhanced performance to examine the influence of stiffener depth, stiffener position, debonding length and aspect ratio subjected to non-uniform compressive in-plane edge load under hygrothermal conditions.

2 Theory and finite element modelling

The mathematical model of the debonded reinforced laminated composite plate is discussed here. The current study is carried out on a plate of size $a \times b \times h$, attached with a T-stiffener at the lower surface of a plate, as presented in Fig. 1a in the cartesian coordinate system (x-y-z). The stiffener has a flange of $b_f \times t_f$ and web of $t_w \times d_w$. The total depth of the stiffener is denoted by d_s (i.e. $d_s = t_f + d_w$). Also, in the current study, the thickness of the flange (t_f) is considered same as the web width (t_w) and is presented as b_s. The current investigation uses the FE technique to study the debonded stiffened plate's buckling capacity. With FE technique, the plate and stiffener are modelled independently, and by using compatibility conditions, the plate and beam elements are tied together. As T-stiffener is used in the present work, the plate and the flange of the stiffener are modelled employing a 9-noded isoparametric heterosis element, while the stiffener web uses a 3-noded isoparametric beam element. The square mesh is adopted for the plate and the stiffener flange, as shown in Fig 2a. Further, by lining up the stiffener flange with the nodal line of the plate element, the stiffener is attached to the plate. Further, the stiffener web is connected to the stiffener flange along the central nodal line of the flange, as delineated in Fig. 1c. The buckling examination is conducted on the debonded stiffened plate subjected to uniaxial load along the edge at $x = 0$ and $x = a$, under the impact of hygrothermal environment, as shown in Fig. 2.
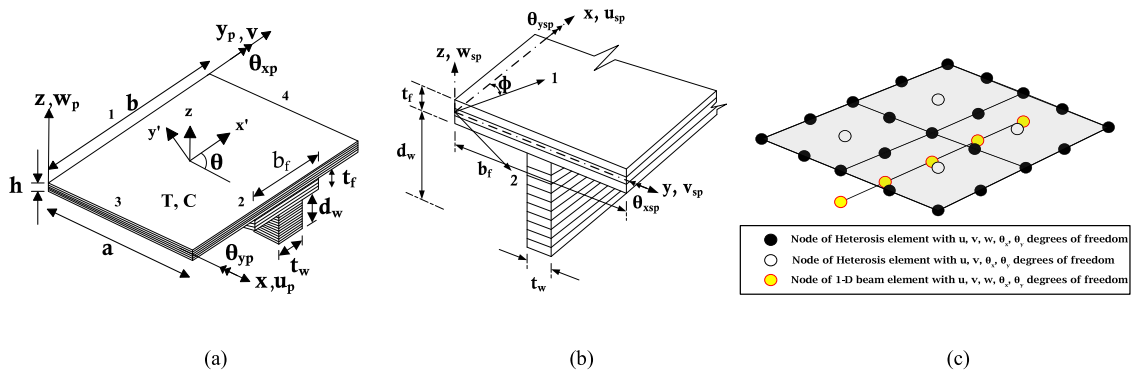

Fig. 1 a Fibre-reinforced stiffened composite plate model, **b** geometry of the T-stiffener and **c** finite element modelling of the T-stiffener
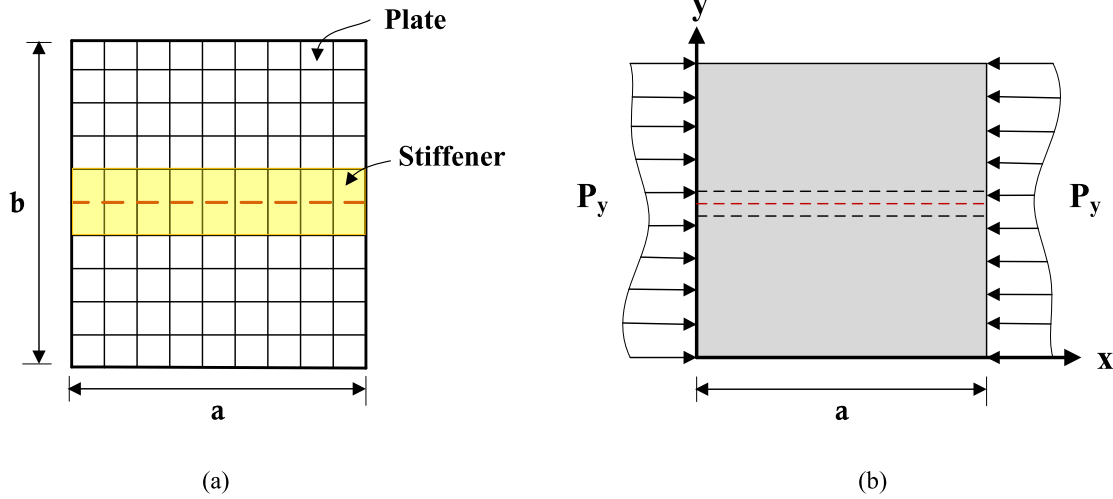
Fig. 2 **a** Meshing scheme of the stiffened plate and **b** stiffened plate configuration with unidirectional stiffener

2.1 Displacement field

In the present study, Reissner–Mindlin hypothesis is employed to model the plate and the stiffener flange by incorporating the shear deformation effect. The displacement field at a point (x, y, z) in terms of mid-plane displacements (u_p, v_p, w_p) and rotations (θ_{xp}, θ_{yp}, 0) is expressed as:

$$\left\{\overline{u_p}(x, y, z), \overline{v_p}(x, y, z), \overline{w_p}(x, y, z)\right\} = \left\{u_p(x, y), v_p(x, y), w_p(x, y)\right\} + z\left\{\theta_{xp}(x, y), \theta_{yp}(x, y), 0\right\} \quad (1)$$

where ($\overline{u_p}$, $\overline{v_p}$) is the primary in-plane displacement and transverse displacement is highlighted by ($\overline{w_p}$).

In the Cartesian coordinate system, Green–Lagrange's strain displacement relation for a plate element is expressed as [29]

$$\varepsilon_{ij} = \frac{1}{2}\left(\frac{\partial u_i}{\partial x_j} + \frac{\partial u_j}{\partial x_i} + \sum_k \frac{\partial u_k}{\partial x_i}\frac{\partial u_k}{\partial x_j}\right) \quad (2)$$

where i, j, and k describes x, y, and z.

The strain–displacement relation, shown in Eq. (2), contains both linear strain and nonlinear strain. Despite the fact that linear analysis is used in the present study, the initial stress stiffness is found by using the Green–Lagrange nonlinear strain displacement term.

2.2 Constitutive model

2.2.1 Constitutive relation of the plate and stiffener flange

The constitutive relation highlighting the resultant stress and moment components {F} to strain element {ε} and resultant stress and moment components induced by the hygrothermal field $\left\{F^N\right\}$ is presented as [30]

$$\{F\} = [C]\{\varepsilon\} - \left\{F^N\right\} \quad (3)$$

In Eq. (3), [C] represents constitutive matrix of laminate [31]. To address the parabolic distribution of shear stress across the plate's depth, a correction factor of 5/6 is utilized in the shear-shear coupling element of constitutive matrix [32].
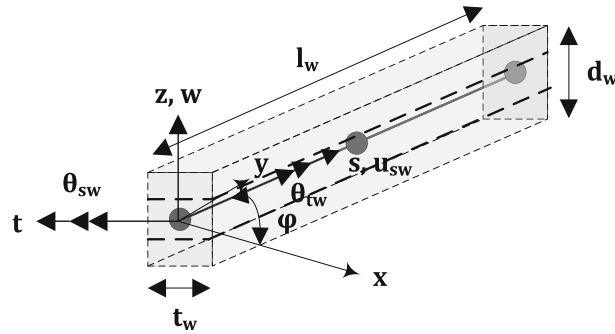
Fig. 3 Geometrical arrangement of the arbitrary oriented laminated beam stiffener

2.2.2 Constitutive modelling of the stiffener web

Consider a stiffener web as a uniform orthotropic laminated beam with a total depth 'd_w', length 'l_w', and width 't_w' in a cartesian coordinates system (x, y, z) angled at φ about the global x-axis, as presented in Fig. 3. On the basis of modified beam theory [33], the displacement field is accorded by

$$\{\overline{u}_{sw}, \overline{v}_{sw}, \overline{w}_{sw}\} = \{u_{sw}, 0, w_{sw}\} + z\{\theta_{sw}, \theta_{tw}, 0\} \tag{4}$$

where, u_{sw} and w_{sw} are the axial and transverse displacements, θ_{sw} and θ_{tw} are bending and torsional rotations about the t- and s-axes, respectively.

The resultant stress and moment with respect to the stiffener's local axis (s- t- z) under the influence of hygrothermal condition is given by

$$\{F_w\} = \left[D^w\right]\{\varepsilon_w\} - \left\{F_w^N\right\} \tag{5}$$

In which $\{F_w\}^T = \left\{N_s^i, M_s^i, M_{st}^i, Q_{sz}^i\right\}^T$ and $\{\varepsilon_w\}^T = \left\{\varepsilon_i^s, \chi_i^s, \chi_i^{st}, \chi_i^{sz}\right\}^T$ are the resultant stress and strain vectors of web, respectively, the resultant force and moment induced by hygrothermal load is highlighted by $\left\{F_w^N\right\}^T = \left\{N_{sN}^i, M_{sN}^i, M_{stN}^i, 0\right\}^T$. The laminated stiffener web's constitutive matrix $[D_w]$ is highlighted extensively by Patel et al. [34]. Kalgutkar et al. [35] thoroughly discuss the beam's detailed formulation by considering the hygrothermal condition. A torsional correction factor proposed by Ugural et al. [37] is employed, which underlies on the web's depth-to-breadth ratio (d_w/t_w). The constitutive matrix's shear-shear coupling components incorporate a shear correction factor suggested by Dharmarajan et al. [36] to expiate the parabolic shear stress distribution along the stiffener's depth.

2.3 Finite element concept

2.3.1 Plate and stiffener flange formulation

This section provides a brief overview of the FE formulation of the stiffened plate. To discretize the plate and stiffener flange, the current investigation considers a 9-noded heterosis element. The elastic stiffness matrix, geometric stiffness matrix due to applied in-plane loads, residual stiffness matrix due to hygrothermal load, mass matrix, and element nodal load vector are determined by employing the minimum potential energy principle, which is described elaborately by Sai Ram et al. [30] and not highlighted here for brevity. The considered formulation was developed for an 8-noded element. However, it is extended to a 9-noded heterosis element for the purposes of this study.

Similarly, the different stiffness and mass matrices for the stiffener flange are obtained by pre-multiplying and post-multiplying the transformation matrix $[T_p]$ and $[T_f]$ with the plate element formulation. The $[T_p]$ is the transformation matrix associated with the orientation of the stiffener flange, and the transformation matrix $[T_f]$ is employed to express the flange's degree of freedom (dof's) in terms of the plate's dof's. This is obtained by implementing the displacement constraints at the plate-flange interface.

2.3.2 Stiffener web formulation

As mentioned in the previous subsection, a 3-noded isoparametric beam element is employed to depict the stiffener's web. The elastic stiffness matrix $[k_{es}]$, the geometric stiffness matrix due to the applied in-plane load $[k_{Gs}]$ and the mass matrix $[m_s]$, for the beam element are obtained by employing Green–Lagrange's strain–displacement term [38], as concisely presented by Rajanna et al. [9] and have not included here for the conciseness purpose.

However, the nodal hygrothermal force vector is written as

$$\{f_w^{HT}\}_j = t_w \int_{l_w} [T_p]_J^T [T_f]_j^T [T_w]_j^T [B_w]_j^T \{F_w^N\}_j dl \tag{6}$$

The web's geometric stiffness matrix due to residual hygrothermal field stresses is outlined as

$$[k_{Gw}^N]_j = t_w \int_{l_w} [T_p]_j^T [T_f]_j^T [T_w]_j^T [G_w^N]_j^T [S_w^N]_j [G_w^N]_j [T_w]_j [T_f]_j [T_p]_j dl \tag{7}$$

in which,

$$[G_w^N] = \begin{bmatrix} \frac{\partial N_{si}}{\partial s} & 0 & 0 & 0 & 0 \\ 0 & 0 & \frac{\partial N_{si}}{\partial s} & 0 & 0 \\ 0 & 0 & 0 & \frac{\partial N_{si}}{\partial s} & 0 \\ 0 & 0 & 0 & 0 & \frac{\partial N_{si}}{\partial s} \\ 0 & 0 & 0 & N_{si} & 0 \end{bmatrix}_{i=1,2,3} \qquad [S_w^N] = \begin{bmatrix} N_s^0 & 0 & M_s^0 & 0 & Q_{sz}^0 \\ 0 & N_s^0 & 0 & 0 & 0 \\ M_s^0 & 0 & \frac{d_s^2}{12}N_s^0 & 0 & 0 \\ 0 & 0 & 0 & \frac{d_s^2}{12}N_s^0 & 0 \\ Q_{sz}^0 & 0 & 0 & 0 & 0 \end{bmatrix} \tag{8}$$

The transformation matrix $[T_w]$ is derived by implementing displacement constraint at the stiffener flange and web interface.

2.3.3 Equation of motion

The stiffened laminated composite plate's equation of motion under the action of in-plane loads exposed to a hygrothermal environment (Fig. 2b) is defined as

$$[M]\{\ddot{\delta}\} + [[K_e] - [K_G^N] - P[K_G]]\{\delta\} = \{0\} \tag{9}$$

where $[K_e]$, $[K_G^N]$, $[K_G]$, and $[M]$ are the elastic stiffness matrix, residual stiffness due to hygrothermal load, geometric stiffness matrix due to in-plane load, and consistent mass matrix, respectively.

The buckling characteristics equation is derived by substituting $\{\ddot{\delta}\} = 0$. Hence, Eq. (9) transforms to

$$[[K_e] - [K_G^N] - P_{cr}[K_G]]\{\delta\} = \{0\} \tag{10}$$

where P_{cr} is the critical buckling load factor of the stiffened plate. Equations (10) illustrate the eigenvalue problem, and $\{\delta\}$ depicting the eigenvectors for the different buckling modes.

2.3.4 Modelling of the debond region with the fictitious spring

Figure 4a depicts the nodal representation of the plate–stiffener flange interface. The parent nodes are cleaved in the delamination or debond region to form dummy nodes that demarcate the delamination or debond. Further, the displacement compatibility condition is employed in the bonded region to define the flange's nodal degrees of freedoms (dofs) in terms of plate dofs. On the other hand, the parent and dummy nodes move independently in the delaminated region. Furthermore, to prevent the dummy node from interpenetrating the parent node, a fictitious spring is introduced between the parent and dummy nodes in the debonded region, as shown in Fig. 4b. Sekine et al. [39] describe the procedure for inserting a fictitious spring between the penetrated node. A three-step procedure is used to implement this method. First, for each pair of overlapped points, a suitable value of $^{ij}k^*$ is found, then the stiffness matrix is modified to include the effect of the new spring, and finally, the eigenproblem is solved.
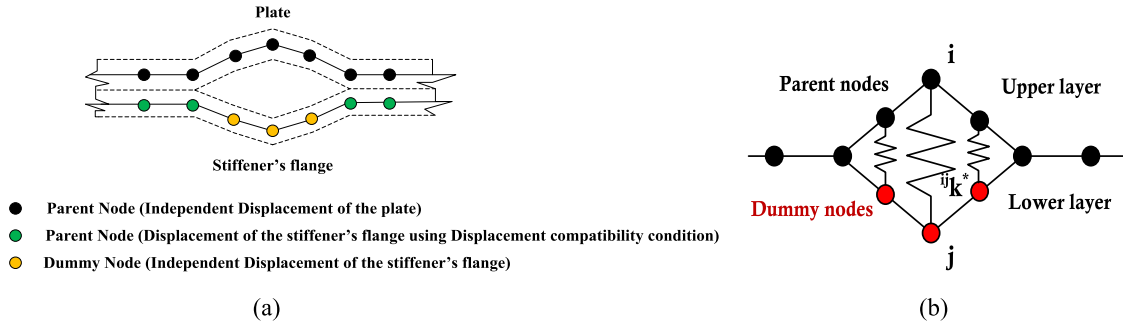
Fig. 4 **a** Nodal representation of the plate-stiffener interface and **b** schematic view of the interface with fictitious spring
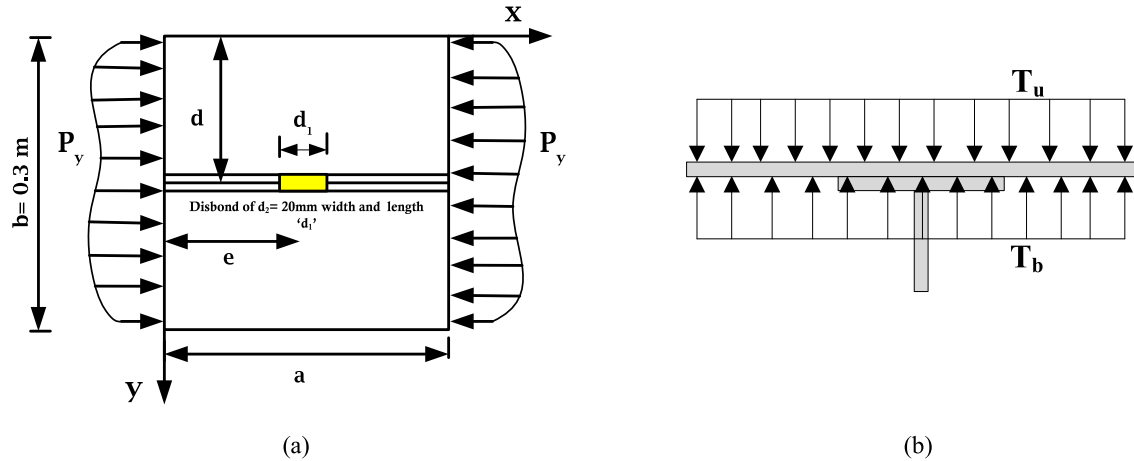

Fig. 5 **a** Schematic representation of the debonded stiffened plate with loading and **b** stiffened plate model with hygrothermal loading variation

The stiffness of the iteratively solved inserted fictitious spring is given by

$$^{ij}k^* = \frac{\left(K_{ii} + K_{ij}\right)P_j - \left(K_{ij} + K_{jj}\right)P_i + \frac{\delta^{ij}}{1+r}\left(K_{ij}^2 - K_{ii}K_{jj}\right)}{\frac{\delta^{ij}}{1+r}\left(K_{ii} + K_{jj} + 2K_{ij}\right)}$$ (11)

3 Problem details and validation studies

3.1 Problem definition

The present investigation considers a debonded T-stiffened composite plate with a centrally placed horizontal stiffener subjected to uniaxial nonuniform edge load along the boundary at $x = 0$ and $x = a$, under hygrothermal environment as displayed in Fig. 5. In the present examination, a thorough width debond is introduced at the interface of plate and stiffener in the central region of the attached stiffener unless otherwise specified. The C^0 continuity FE formulation is developed for the plate and discrete beam element, suited for examining the performance of debonded stiffened plates. The investigation is conducted on a square plate with a dimension $(a = b)$ of 0.3 m and a length-to-thickness ratio (a/h) of 150. The T- stiffener is attached at a distance 'd' from one edge of the plate, and a debond of through width 'd_2' and length 'd_1' is introduced at a distance 'e' from the edge of the plate as shown in Fig. 5a. The hygrothermal load-dependent elastic properties, considered from Parhi et al. [40] work are employed for the stiffened composite plate at different temperatures and moisture conditions, as indicated in Tables 1 and 2, with a density 'ρ' of 1360 kg/m^3.

The present study is conducted on the thin plate with a uniform variation of hygrothermal load along the thickness and across the surface, as shown in Fig. 5b, with reference temperature T_0= 300 K and reference

Table 1 Elastic moduli of carbon/epoxy at various temperatures; $\upsilon_{12} = 0.3$, $G_{13} = G_{12}$, $G_{23} = 0.4G_{12}$, $\alpha_1 = $ -0.3 $\times 10^{-6}$/K and $\alpha_2 = 28.1 \times 10^{-6}$/K. $C = 0.0\%$

Elastic moduli (GPa)	Temperature T (K)					
	300	325	350	375	400	425
E_1	172.5	172.5	172.5	172.5	172.5	172.5
E_2	6.9	6.17	5.81	5.45	5.08	4.9
G_{12}	3.45	3.45	3.16	2.88	2.73	2.59

Table 2 Elastic moduli of carbon/epoxy at various moisture concentrations; $\upsilon_{12} = 0.3$, $G_{13} = G_{12}$, $G_{23} = 0.4G_{12}$, $\beta_1 = 0$ and $\beta_2 = 0.44$. $T = 300$ K

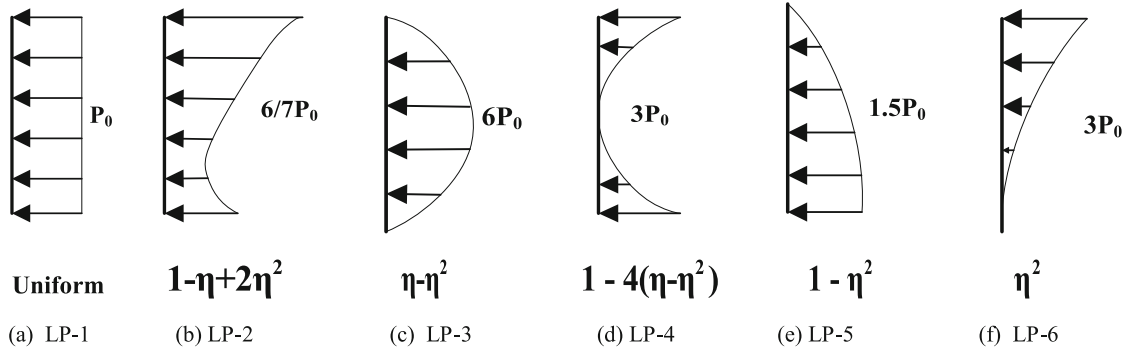| Elastic moduli (GPa)	Moisture concentration, $C\%$					
	0.25	0.50	0.75	1.00	1.25	1.50
E_1	172.5	172.5	172.5	172.5	172.5	172.5
E_2	6.72	6.54	6.36	6.17	6.17	6.17
G_{12}	3.45	3.45	3.45	3.45	3.45	3.45

Fig. 6 Different loading patterns

moisture $C_0 = 0.0\%$ except as otherwise specified. The analysis is performed such that the volume of the attached T-stiffener is one-tenth the volume of the considered plate, irrespective of the plate's size. In the study, a stiffener depth-to-width ratio (d_s/b_s) of 4 is maintained unless otherwise specified. The present study is being conducted on the three hygrothermally stable laminate schemes that are considered based on the observation of earlier researchers. The lamina scheme $(\theta/(90-\theta))_s$ is the configuration that induces equal normal non-mechanical stress resultants and zero non-mechanical shear and moment resultants [41]. The lamina scheme with the better shear extension coefficient is $(22.5/-67.5)_s$, while the lamina scheme with the optimal bending stiffness and compliance is $(77.5/-12.5)_s$ [42].

In addition, six different types of compressive nonuniformly varying loading patterns are considered, as shown in Fig. 6. The term $\eta = y/b$ (loading edge distance) appears in the quadratic equation of load variation. The buckling parameter are compared for different loading patterns by adjusting the loading intensity such that the total applied load equals P_0b. The analysis in this work is performed in three phases. Initially, a stress analysis induced by hygrothermal loading is carried out. Following that, a pre-buckling analysis is done to find the in-plane stress distribution within the plate element as a result of mechanical loading. Finally, the determined in-plane stresses are used to evaluate the critical buckling load. It is worth noting that two types of edge constraints are employed- one for the stress analysis due to hygrothermal loading and the other for the pre-buckling and buckling analysis. Detailed displacement conditions along the boundary have been presented by Kalgutkar et al. [35] and have not been presented for brevity.

The non-dimensional buckling load is expressed as

$$\gamma_{cr} = \frac{P_{cr}b^2}{E_2^{T_{ref}}h^3} \tag{12}$$

Table 3 A validation study of buckling load (P_{cr}) results of the delaminated stiffened composite plate

P_{cr} (N/m)	$\delta/a = 0$	$\delta/a = 0.2$	$\delta/a = 0.4$	$\delta/a = 0.6$
Present	6.05	6.03	5.94	5.74
Castro et al. [43]	6.00	5.96	5.85	5.61

$E_{11} = 142.5$ GPa, $E_{22} = E_{33} = 8.7$ GPa, $G_{12} = 5.1$ GPa, $\upsilon_{12} = 0.28$. a/b = 0.5, b/b_b = 5

Table 4 Stability performance of the hinged plate at the moisture of 0.1% and temperature of 325 K

a/b	a/t	$(0/90)_s$	Moisture $C = 0.1\%$	Temperature $T = 325$ K
1	100	Sai Ram et al. [30]	0.6099	0.4488
		Whitney et al. [44]	0.6091	0.4477
		Present (9- NHE)	0.6081	0.4462
		Present (ABAQUS CAE)	0.6080	0.4461

where γ_{cr} is the non-dimensional buckling load, and P_{cr} highlights the critical buckling load factor of the plate. $E_2^{T_{ref}}$ connotes the transverse modulus of elasticity at reference hygrothermal load.

3.2 Validation studies

Comparison studies are essential for ascertaining the accuracy and efficiency of various matrices associated with analysing the delaminated plate's buckling characteristics. The elastic stiffness matrix and the geometric stiffness matrix are validated by comparing the buckling study results of the current model with classical/numerical solutions. Further, the investigation performed under the hygrothermal environment is validated with the previously available literature on the hygrothermal effect to ascertain the veracity of the formulation of the residual stress matrix.

3.2.1 Validation studies of the debonded reinforced plate under the action of mechanical loading

To validate the model consisting of the debond between the plate and stiffener, which is the interest of the current problem, a comparison study for the buckling behaviour is conducted. The buckling responses are compared to ascertain the elastic stiffness matrix and geometric stiffness matrix formulation. The debonded stiffened composite plate's buckling analysis is carried, and the findings is presented in Table 3 along with the outcomes of Castro et al. [43]. Castro et al. [43] conducted the analysis using a semi-analytical approach to model the debonded stiffened plate, and the entire stiffened plate was modelled using a plate element. From the study, it is noticed that there is a slight variation in the buckling study findings estimated from the current model with the semi-analytical model. This minor deviation might be due to the penetration of the node in the semi-analytical model. Therefore, from the analysis, it is noticed that current findings closely agree with the available literature. Hence, the current formulation can be employed for further studies.

3.2.2 Validation studies of the unreinforced plate subjected to thermomechanical loading

In addition, the residual stiffness matrix due to non-mechanical loading formulation is substantiated by conducting a stability study on the $(0/90)_s$ laminated plate exposed to a moisture concentration of 0.1%, and 325 K temperature. The findings are shown in Table 4 and validated with the results of Sai Ram et al. [30], Whitney et al. [44], and the outcomes obtained from ABAQUS CAE employing S8R5 elements. The findings of the current study are consistent with the available literature's outcome.

4 Parametric investigation on buckling performance of delaminated stiffened composite plates subjected to non-uniform edge load under hygrothermal environment

This segment outlines different case studies performed to demonstrate the impact of several parameters on the buckling capacity of the reinforced plate debonded at the plate-stiffener interface subjected to hygrothermo-mechanical loads. The present research focuses on a square plate with a ratio of thickness-to-width (*b/h*) of
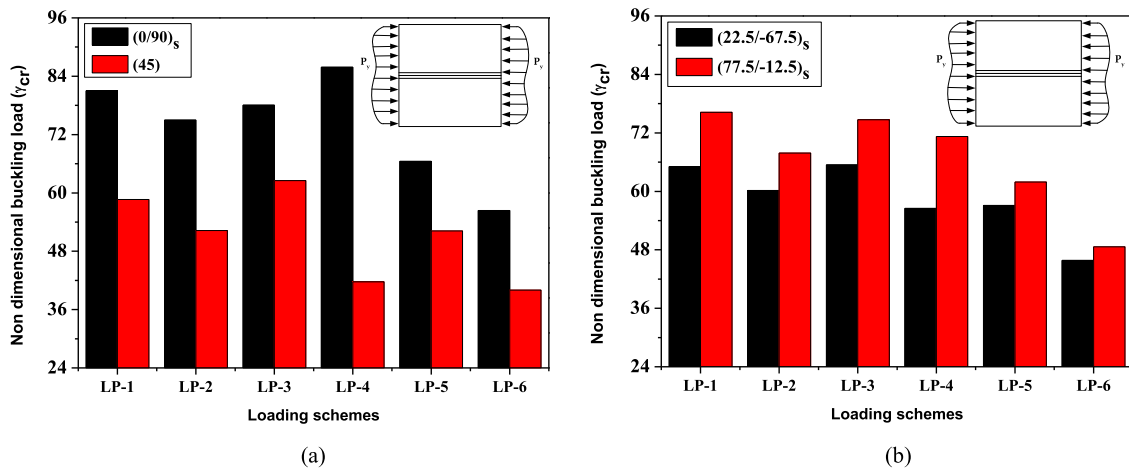
Fig. 7 Influence of the lamina schemes and loading pattern on the buckling strength of the laminated stiffened composite plate

150, except as otherwise provided. The stiffener has a depth-to-width ratio (d_s/b_s) of 4, with fibres lined along the stiffener's axis. Irrespective of the plate's size, the attached stiffener's volume is one-tenth of the volume of the considered plate, and the width of the stiffener web (t_w) is considered to be equal to the thickness of the stiffener flange (t_f).

As previously stated, the investigation is initially conducted to assess the buckling strength of the bonded stiffened plate under the impact of various non-uniform edge loads for different lamina schemes to determine a stiffened plate with a suitable lamina scheme and loading pattern that has enhanced buckling capacity. The obtained stiffened plate is further investigated for different parameters under hygrothermal loading conditions.

4.1 Impact of lamina schemes and loading patterns on the buckling capacity of the stiffened laminated composite plate

In this section, a preliminary study is performed to comprehend the stability performance of the stiffened plate for various lamina schemes and loading patterns. This research aims to identify stiffened plates with improved buckling capacity so that further parameter studies can be performed on it under hygrothermal conditions. In the present study, debond is not introduced in the stiffened plate, and the stiffener parallel to the length of the plate (x-axis) is positioned at the centre of the plate. The stiffener has a d_s/b_s of 4. As previously discussed, the study is performed by subjecting the plate to six different loading patterns with four lamina schemes. Figure 7 presents the outcome of the buckling study. From the investigation, it is noted that among the different lamina scheme plates subjected to various loading patterns, the plate with $(0/90)_s$ lamina scheme under the action of inverse parabolic edge load (LP-4) has enhanced stability. On the other hand, the plate with 45° oriented plies has the least buckling capacity. It is interesting to note that irrespective of the loading scheme, the sequence of the lamina scheme with reduced stability is as $(0/90)_s > (77.5/-12.5)_s > (22.5/-67.5)_s > (45)_s$.

As a result, the stiffened plate with $(0/90)_s$ lamina scheme under the action of LP-4 load is taken into account in the subsequent parametric studies. It is worth noting that the lamina scheme significantly affects the plate's stability under the impact of in-plane load. Apart from this, it can be highlighted that when a large portion of higher intensity load is applied on the plate along the lamina direction, the plate's stability will be minimal. For $(0/90)_s$ laminated plate, enhanced stability is observed when the plate is applied with LP-4 pattern (load intensity is highest at the corner) whereas, the $(45)_s$ plies stiffened plate subjected to LP-3 pattern (load intensity is significant at the central region) has the enhanced stability when compared to other loading cases.
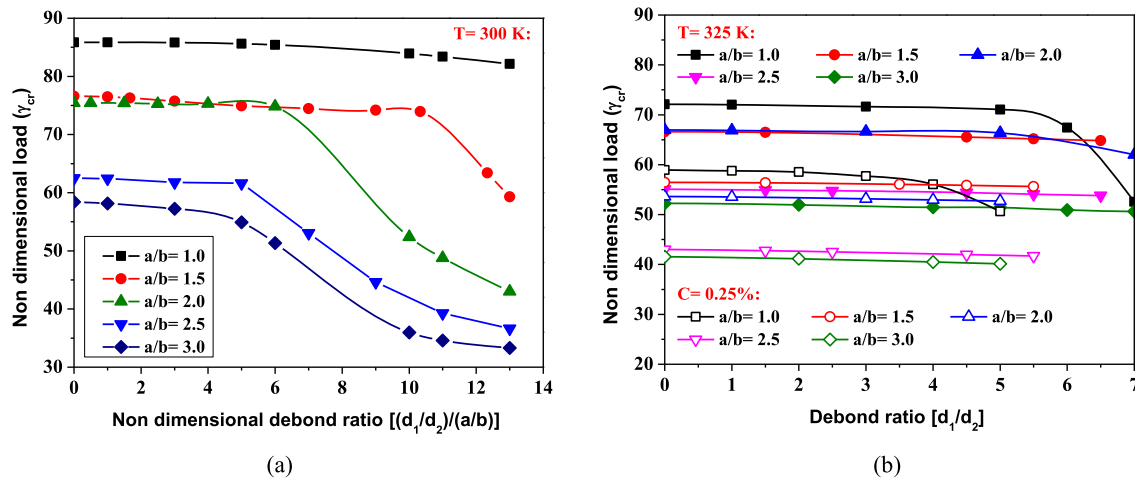
(a)   (b)

Fig. 8 Effect of debonding length on the buckling strength of the debonded stiffened composite plate in the **a** absence of hygrothermal load and **b** presence of hygrothermal load

4.2 Impact of various parameters on the buckling performance of the debonded reinforced composite plate under hygrothermal environment

An investigation is undertaken in the preceding subsection to figure out the stable scheme of the T-stiffened laminated plate based on the stability behaviour and discovered that $(0/90)_s$ plate applied to LP-4 loading has an enhanced buckling capacity. Further subsequent investigation is carried out on the $(0/90)_s$ T- stiffened composite plate provided with through width debond at the plate-stiffener interface to study the stability behaviour under the influence of various parameters exposed to uniform hygrothermal loading. In all the considered parametric studies, only one unidirectional T-stiffener is attached at the plate's bottom surface.

4.2.1 Impact of debonding length on the buckling strength of the debonded reinforced plate for different aspect ratios of the plate

In this subsection, an investigation is conducted to study the debonded stiffened plate's stability under hygrothermal loading conditions. In the present work, the width (b) and thickness (h) of the plate is retained to 300 mm and 2 mm, respectively, and only the plate's length (a) varies depending on the required aspect ratio (a/b). It is important to note that the volume of the stiffener is equal to one-tenth of the plate's volume, irrespective of the plate's aspect ratio. A through width debond 'd_2' of 20 mm is introduced in the central region of the attached stiffener, and the length of the debond 'd_1' varies depending on the debond ratio (d_1/d_2). The analysis is performed at the reference temperature, 325 K temperature and 0.25% moisture, and the findings are shown in Fig. 8. From the investigation, it is seen that with the increase in the plate's aspect ratio, the buckling load of the plate drops significantly due to the loss in the plate's stiffness irrespective of the hygrothermal conditions. Figure 8a shows that as the plate is exposed to reference temperature or moisture, the plate's buckling capacity drops by a small amount at lower d_1/d_2 values. Further, as the length of the debond rises, a sudden drop in the buckling load is noticed. The buckling load drop is quite significant in the higher aspect ratio plate due to the loss of stiffness because of the longer panel's length and larger debonding size.

The stiffened plate's buckling strength abates significantly as exposed to hygrothermal load. This behaviour is quite noticeable in the case of a lower aspect ratio plate. However, a sudden drop in the buckling capacity occurs at a short debond length. This is because, along with the reduction in mechanical buckling load, the critical hygrothermal load (i.e. the non-mechanical load at which the plate loses its stability) reduces substantially as the debonded length increases.

For a better understanding on the debonded stiffened plate's stability, the von Mises stress plots are presented. Figure 9 depicts a stress plot of a rectangular stiffened plate with an aspect ratio of 3 for different debonding lengths subjected to $T = 300$ K. From the plot, it is observed that the stress intensity drops with the enhancement in the debonding size. Furthermore, at the small size debond, the stress is concentrated at the debonding edge in a smaller region. On the other hand, as the debonding size increases, the stress is highly
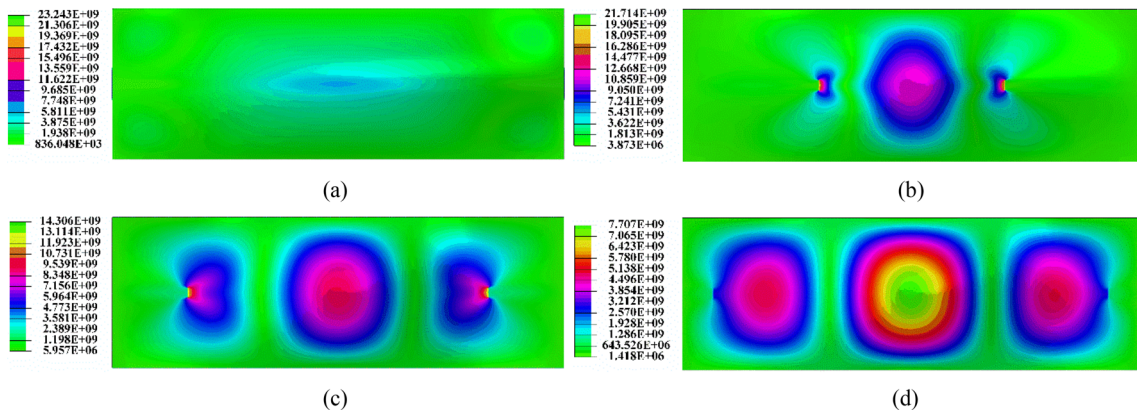
Fig. 9 Von Mises stress plot of the rectangular stiffened plate of an aspect ratio of 3 with the debond length of **a** 0 mm, **b** 300 mm, **c** 600 mm, and **d** 780 mm
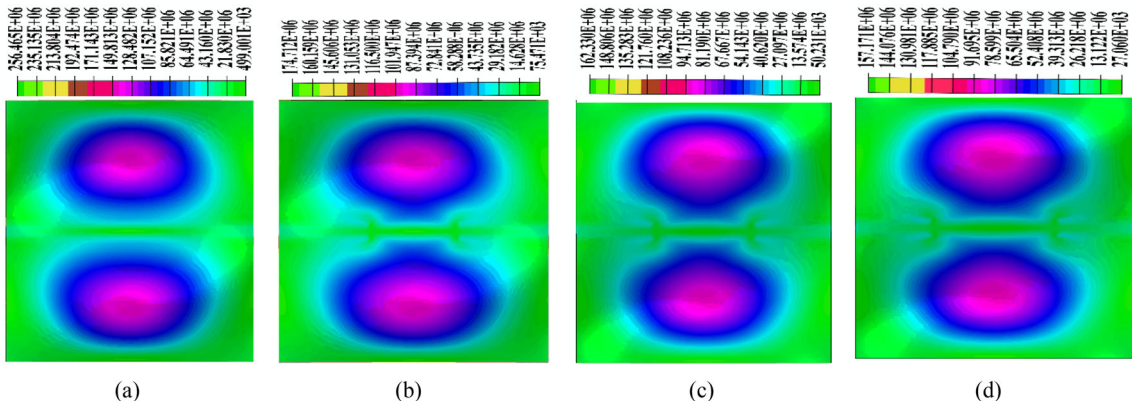

Fig. 10 Von Mises stress plot of a square reinforced plate with the debond length of **a** 0 mm, **b** 100 mm, **c** 120 mm, and **d** 140 mm subjected to a temperature of 325 K

focused in the central region of the debond in the plate. Figure 10 depicts the stress plot of a debonded square plate exposed to a temperature of 325 K. The introduction of hygrothermal load results in a drastic reduction in the stress induced in the structure, and the intensity of the stress also decreases as the debonding length increases. Additionally, as the debonding size enhances, a small amount of stress is focussed in the debonded region. Hence, it is noticed that larger the stress induced in the structure, greater is the plate's buckling strength.

4.2.2 Impact of stiffener depth on the buckling behaviour of the debonded stiffened plate

The current segment outlines the investigation that considers the effect of stiffener depth on the stability behaviour of the plate under hygrothermal load. In this work, the volume of the attached stiffener is retained to one-tenth of the volume of the plate, and accordingly, the width (t_w) and web's depth (d_w) are adjusted. Furthermore, the flange thickness (t_f) is equal to the stiffener web width (t_w). The stiffener depth-to-width ratio (d_s/b_s) of one is an instance of a plate attached to a spread stiffener. In the current investigation, a 60 mm × 20 mm debond is introduced in the central region of the attached stiffener. The investigation is performed at varying moisture concentrations and temperature intensities, and the outcomes are shown in Fig. 11. It can be noted that at the lower temperature up to 350 K, the buckling load decreases marginally with enhancing the d_s/b_s ratio. This drop might be due to a reduction in the flange thickness with the rise in d_s/b_s to retain a constant stiffener volume. With the temperature increase, the plate's buckling load increases abruptly with the d_s/b_s ratio. This performance is due to a drastic loss of the plate's stiffness at lower d_s/b_s than in the stiffened plate with a higher d_s/b_s value. This shows that at the higher value of d_s/b_s (i.e. at the greater stiffener depth), the exposed temperature has a marginal influence on the plate's stability compared with a plate with a lower depth of stiffener. Similarly, debond significantly impacts plate stability at lower d_s/b_s values.
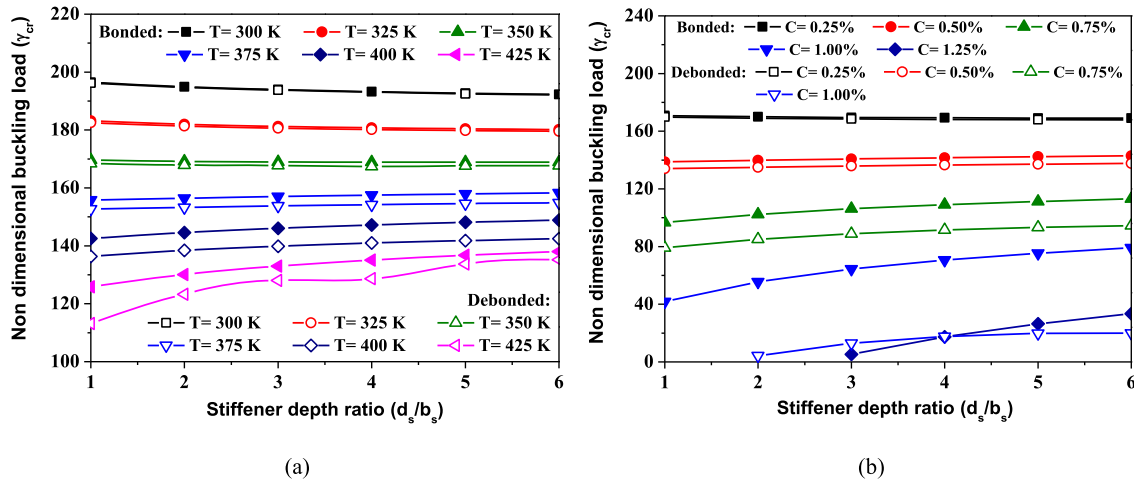
Fig. 11 Effect of stiffener depth on the buckling strength of bonded and debonded stiffened laminated plates under the impact of **a** temperature and **b** moisture

On the other hand, Fig. 11b highlight the buckling behaviour of stiffened plate under moisture effect. A similar trend is observed in the buckling behaviour, comparable to the temperature effect on buckling capacity. At lower moisture content up to 0.5%, the plate's stability marginally reduces with increasing stiffener depth ratio. However, at higher moisture concentrations, the buckling capacity increases significantly as the d_s/b_s ratio rises. Contrarily, the panel's stability reduces significantly with debonding with the rise in the moisture concentration. Also, the drop in the plate's buckling capacity caused by debonding is higher at the lower depth of the stiffener due to the increase in the flange thickness. It can also be noticed that moisture extensively affects the plate's buckling behaviour more than the temperature.

4.2.3 Effect of stiffener position on the buckling performance of the debonded stiffened plate for different stiffener depths

This study examined the effect of the stiffener position on the debonded stiffened plate's stability under LP-4 pattern. In the current examination, a through width debond of length 60 mm is introduced in the plate centre, irrespective of the stiffener position. In the study, the stiffener position 'd' is measured from the plate edge to the stiffener's central line. The analysis is performed at the reference temperature, 400 K temperature and 0.75% moisture and the findings are shown in Fig. 12. From the finding, it is reported that at $T = 300$ K, there is a slight drop in the plate stability as the eccentricity of the stiffener 'd' is increased from 30 to 70 mm from the edge. On the other hand, as the stiffener is attached towards the centre of the plate, i.e. $d = 150$ mm, the plate's stability increases abruptly. This abrupt enhancement in the plate's buckling load is significantly noticed in the lower stiffener depth-to-width ratio plate. Although a quite minimal significance of debonding on the plate's stability is noted, a considerable drop in buckling load is noticed in the case of the centrally placed stiffener, irrespective of the d_s/b_s ratio.

In contrast, under hygrothermal environment, a contrary behaviour is observed. The plate's stability initially increases as the stiffener is placed from the edge up to the 90 mm distance from the edge. Furthermore, placing the stiffener in the centre reduces the buckling load dramatically. It is also observed that when the stiffener is placed at the edge, the stiffener depth ratio does not play a vital role on the stability and only debonding slightly reduces the buckling capacity. However, as the stiffener is positioned towards the plate's centre, the stability substantially increases with the stiffener depth ratio rise. Also, with the introduction of debonding, the plate's stability degrades with hygrothermal exposure, irrespective of the d_s/b_s ratio. On the other hand, a similar performance is noticed in the plate affected by moisture as it is marked in the plate under thermal environment. However, the plate's stability substantially degrades when the stiffener is placed in the plate's central region, and it is predominantly observed in the plate with a lower d_s/b_s ratio. Therefore, one can conclude that centrally placed stiffened plates with lower stiffener depth are less stable under exposure to hygrothermal load.

The von Mises stress plots of the debonded reinforced plate with d_s/b_s of 6 for the varying position of the stiffener subjected to reference temperature and moisture concentration of 0.75% are manifested in Figs. 13
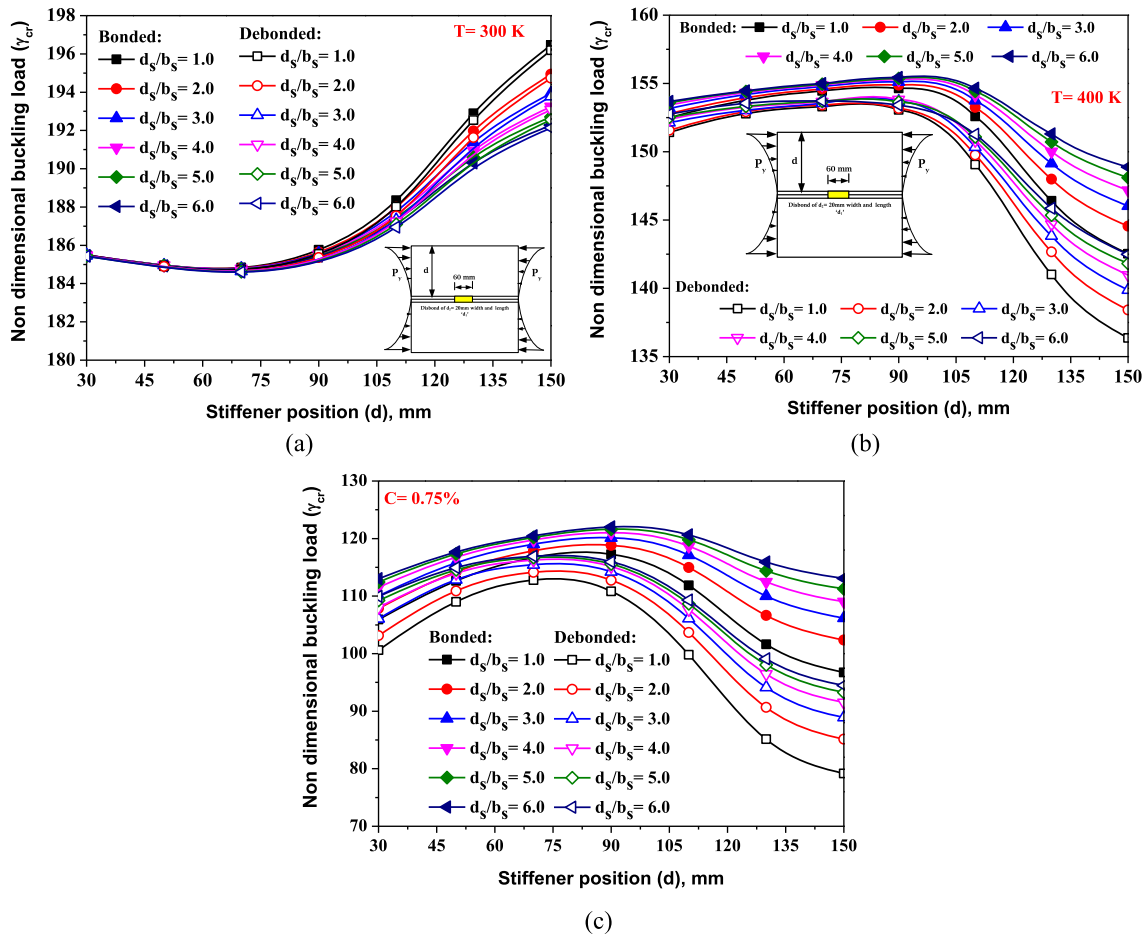
Fig. 12 Influence of stiffener position on stiffened plate's stability under the impact of hygrothermal load of **a** $T = 300$ K, **b** $T = 400$ K, and **c** $C = 0.75\%$ for different stiffener depth ratios

and 14, respectively. It is seen that when the stiffener is attached towards the edge of the plate, a considerable amount of stress is concentrated towards the opposite edge of the plate at a reference temperature. However, there is a small rise in the stress intensity when the stiffener is attached slightly closer to the plate's centre, indicating a marginal drop in the buckling capacity, as shown in Fig. 12a. Furthermore, moving the stiffener closer to the centre of the plate gradually increases the stress intensity. Also, the stress is equally distributed across either region of the stiffener for a centrally positioned stiffened plate, indicating improved stability. On the contrary, when the plate is subjected to moisture, the stress intensity reduces drastically, indicating stability deterioration. Here, the stress is highly concentrated towards the edge of the plate, which is contrary to the plate's behaviour under reference conditions. The stress intensity initially increases and then drops as the stiffener is moved from the edge to the plate's centre, indicating a similar stability performance as seen in Fig. 12c. This indicates that under the reference condition, the stress is focussed on the central region of the plate, indicating enhanced stability, while under moisture exposure, the stress is highly concentrated towards the edge, pointing to lower stability.

5 Concluding remarks

In this study, the authors have attempted to investigate the impact of thermal and humidified conditions on the stability behaviour of a debonded T-stiffened composite plate by applying a generalized FE framework in a MATLAB environment. Unlike previous studies that used a plate element to model the stiffener, this study considers modelling the stiffener web with a beam element, which reduces the computational cost. Four types of hygrothermally stable lamina schemes and six different loading patterns are considered. The key objective
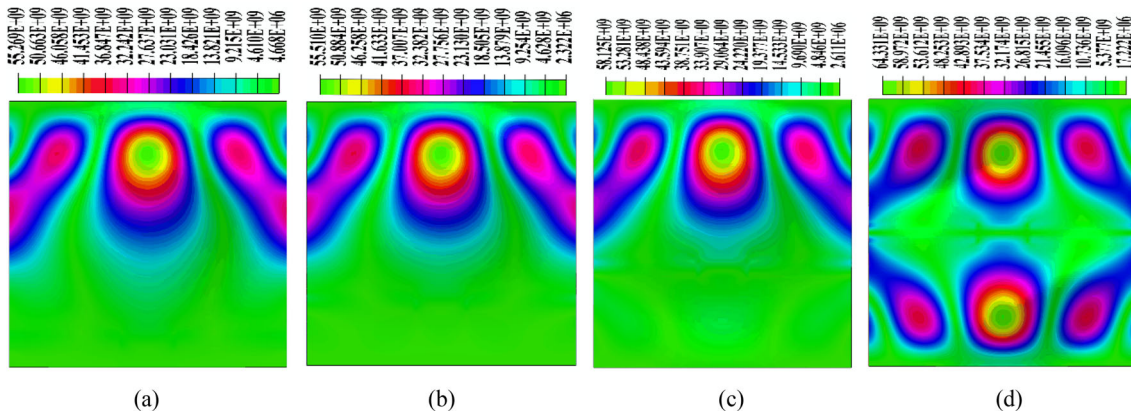
Fig. 13 Von Mises stress plot of a square stiffened plate provided with a central debond length of 60 mm with a stiffener placed at a distance of **a** 30 mm, **b** 70 mm, **c** 110 mm, and **d** 150 mm from the edge at a reference temperature
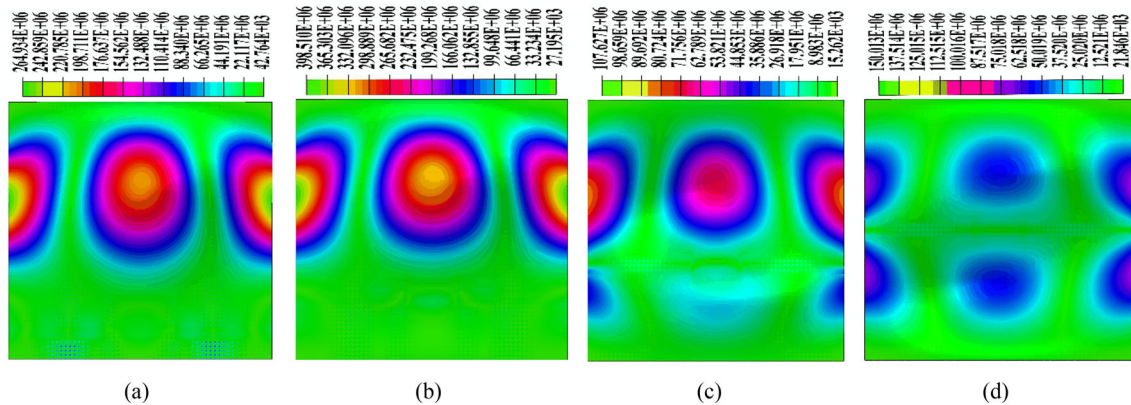

Fig. 14 Von Mises stress plot of a square stiffened plate with a central debond length of 60 mm with a stiffener placed at a distance of **a** 30 mm, **b** 70 mm, **c** 110 mm, and **d** 150 mm from the edge exposed at 0.75% moisture concentration

of the current research is to determine a stiffened composite plate with a specific lamina and loading pattern that has enhanced buckling capacity and further to inspect the impact of various parameters in the presence and absence of debonding exposed to hygrothermal conditions under the action of non-uniform edge loads. Extensive parametric investigations are conducted, and the prominent outcomes are summarized as follows:

i. The T-stiffened composite plate with $(0/90)_s$ lamina scheme under the action of inverse parabolic loading (LP-4) has enhanced buckling capacity.

ii. As the hygrothermal load intensity rises, the buckling strength of the higher aspect ratio plate abates significantly at a larger size of debonding.

iii. The stability degrades with an increase in the stiffener depth ratio (d_s/b_s) at a lower magnitude of the hygrothermal load. On the contrary, the plate's stability increases abruptly with the enhancement in stiffener depth-to-width ratio (d_s/b_s) at higher hygrothermal load intensity. However, at the lower stiffener depth ratio (d_s/b_s), hygrothermal loading and debond significantly degrade the plate's stability.

iv. At the reference hygrothermal load, the buckling load of the plate initially degrades as the stiffener is placed from the edge up to a certain distance towards the centre of the plate. Further, as the stiffener is positioned towards the plate's centre, the plate stability enhances significantly.

v. Under the exposure of hygrothermal loading, contrary buckling behaviour is noticed. The plate's buckling capacity initially increases, and then a gradual drop is seen as the stiffener is placed from the edge to the plate's centre.

vi. When a stiffener is attached at the plate centre, the stability of the plate with a lower stiffener depth ratio (d_s/b_s) (i.e. plate attached to spread stiffener) increases significantly at the reference hygrothermal load. On the contrary, the stability of the lower stiffener depth ratio (d_s/b_s) plate drops substantially in the presence of hygrothermal loading.

From the parametric investigation, it can be stated that several parameters remarkably impact the stability performance of the stiffened plates under environmental conditions. Also, one can draw the conclusion that moisture considerably influences the stiffened plate's behaviour more than the temperature. Finally, it can be inferred that the current model has an advantage in reducing the computational cost due to the partial use of 1-D element for the stiffener. However, the current FE model is only capable of handling non-progressive damage during loading. This problem can be solved by using other techniques to model the progressive debonding while taking into account the stress fields along with displacement fields.

Declarations

Conflict of interest The authors declare that they have no known competing financial interests or personal relationships that could have appeared to influence the work reported in this paper.

References

1. Garg, A., Chalak, H.D.: A review on analysis of laminated composite and sandwich structures under hygrothermal conditions. Thin-Wall. Struct. **142**, 205–226 (2019). https://doi.org/10.1016/j.tws.2019.05.005
2. Reddy, J.N., Phan, N.D.: Stability and vibration of isotropic, orthotropic and laminated plates according to a higher-order shear deformation theory. J. Sound Vib. **98**(2), 157–170 (1985). https://doi.org/10.1016/0022-460X(85)90383-9
3. Zenkour, A.M.: Buckling and free vibration of elastic plates using simple and mixed shear deformation theories. Acta Mech. **146**(3), 183–197 (2001). https://doi.org/10.1007/BF01246732
4. Ghannadpour, S.A.M., Najafi, A., Mohammadi, B.: On the buckling behavior of cross-ply laminated composite plates due to circular/elliptical cutouts. Compos. Struct. **75**(1), 3–6 (2006). https://doi.org/10.1016/j.compstruct.2006.04.071
5. Qin, X., Xiang, J., He, X., Shen, Y., Chen, W., Peng, L.X.: Buckling analysis of skew and circular stiffened plates using the Galerkin meshless method. Acta Mech. **233**(5), 1789–1817 (2022). https://doi.org/10.1007/s00707-022-03191-w
6. Kumar, Y.: The Rayleigh-Ritz method for linear dynamic, static and buckling behavior of beams, shells and plates: a literature review. J. Vib. Control **24**(7), 1205–1227 (2017). https://doi.org/10.1177/1077546317694724
7. Jaunky, N., Knight, N.F., Ambur, D.R.: Formulation of an improved smeared stiffener theory for buckling analysis of grid-stiffened composite panels. Compos. B Eng. **27**(5), 519–526 (1996). https://doi.org/10.1016/1359-8368(96)00032-7
8. Leissa, A.W., Kang, J.-H.: Exact solutions for vibration and buckling of an SS-C-SS-C rectangular plate loaded by linearly varying in-plane stresses. Int. J. Mech. Sci. **44**(9), 1925–1945 (2002). https://doi.org/10.1016/S0020-7403(02)00069-3
9. Rajanna, T., Banerjee, S., Desai, Y.M., Prabhakara, D.: Effect of reinforced cutouts and ply-orientations on buckling behavior of composite panels subjected to non-uniform edge loads. Int. J. Struct. Stab. Dyn. **18**(04), 1850058 (2018). https://doi.org/10.1142/S021945541850058X
10. Liu, N., Yu, W., Hodges, D.H.: Mechanics of structure genome-based global buckling analysis of stiffened composite panels. Acta Mech. **230**(11), 4109–4124 (2019). https://doi.org/10.1007/s00707-018-2339-4
11. Huang, S., Qiao, P.: A novel semi-analytical method for buckling analysis of stiffened laminated composite plates. Thin-Wall. Struct. **148**, 106575 (2020). https://doi.org/10.1016/j.tws.2019.106575
12. Kalgutkar, A.P., Banerjee, S., Rajanna, T.: Effect of elliptical cutouts on buckling and vibration characteristics of stiffened composite panels under non-uniform edge loads. Mech. Based Design Struct. Mach. **51**, 1–15 (2021). https://doi.org/10.1080/15397734.2021.1999266
13. Kalgutkar, A.P., Banerjee, S., Rajanna, T.: Optimum arrangement of stiffener on the buckling behaviour of stiffened composite panels with reinforced elliptical cutouts subjected to non-uniform edge load. Steel Compos. Struct. **42**(4), 427–446 (2022). https://doi.org/10.12989/scs.2022.42.4.427
14. Chattopadhyay, B., Sinha, P.K., Mukhopadhyay, M.: Finite element analysis of blade-stiffened composite plates under transverse loads. J. Reinf. Plast. Compos. **12**(1), 76–100 (1993). https://doi.org/10.1177/073168449301200105
15. Li, D., Tang, G., Zhou, J., Lei, Y.: Buckling analysis of a plate with built-in rectangular delamination by strip distributed transfer function method. Acta Mech. **176**(3), 231–243 (2005). https://doi.org/10.1007/s00707-004-0206-y
16. Shao, Q., He, Y.T., Zhang, T., Zhang, H.W., Kang, Q.S.: Simulation of compress buckling performance of composite stiffened panel. Appl. Mech. Mater. **184–185**, 1189–1193 (2012). https://doi.org/10.4028/www.scientific.net/AMM.184-185.1189
17. Yap, J.W.H., Scott, M.L., Thomson, R.S., Hachenberg, D.: The analysis of skin-to-stiffener debonding in composite aerospace structures. Compos. Struct. **57**(1), 425–435 (2002). https://doi.org/10.1016/S0263-8223(02)00110-1
18. Ovesy, H.R., Fazilati, J.: Buckling and free vibration finite strip analysis of composite plates with cutout based on two different modeling approaches. Compos. Struct. **94**(3), 1250–1258 (2012). https://doi.org/10.1016/j.compstruct.2011.11.009
19. Al-Khaleefi, A.M., Kabir, H.R.H.: On the thermal buckling response of shear-flexible all-edge clamped rectangular plates. J. Vib. Control **9**(5), 495–506 (2003). https://doi.org/10.1177/1077546303009005001
20. Cui, D., Hu, H.: Thermal buckling and natural vibration of a rectangular thin plate with in-plane stick-slip-stop boundaries. J. Vib. Control **22**(7), 1950–1966 (2014). https://doi.org/10.1177/1077546314546394

21. Panda, H.S., Sahu, S.K., Parhi, P.K.: Buckling behavior of bidirectional composite flat panels with delaminations in hygrothermal field. Acta Mech. **226**(6), 1971–1992 (2015). https://doi.org/10.1007/s00707-014-1280-4
22. Nikrad, S.F., Asadi, H., Akbarzadeh, A.H., Chen, Z.T.: On thermal instability of delaminated composite plates. Compos. Struct. **132**, 1149–1159 (2015). https://doi.org/10.1016/j.compstruct.2015.07.019
23. Kumar, R., Ramachandra, L.S., Banerjee, B.: Semi-analytical approach for thermal buckling and postbuckling response of rectangular composite plates subjected to localized thermal heating. Acta Mech. **228**(5), 1767–1791 (2017). https://doi.org/10.1007/s00707-016-1797-9
24. Amoushahi, H., Goodarzian, F.: Dynamic and buckling analysis of composite laminated plates with and without strip delamination under hygrothermal effects using finite strip method. Thin-Wall. Struct. **131**, 88–101 (2018). https://doi.org/10.1016/j.tws.2018.06.030
25. Mondal, S., Ramachandra, L.S.: Stability and failure analyses of delaminated composite plates subjected to localized heating. Compos. Struct. **209**, 258–267 (2019). https://doi.org/10.1016/j.compstruct.2018.10.087
26. Xia, F., Xue, J., He, Z., Yao, S., Jin, F., Yuan, H.: Buckling and post-buckling of delaminated Reissner-Mindlin panels subjected to hygro-thermal-mechanical multi-field loading. Thin-Wall. Struct. **162**, 107583 (2021). https://doi.org/10.1016/j.tws.2021.107583
27. Chamis, C.C., Sendeckyj, G.P.: Critique on theories predicting thermoelastic properties of fibrous composites. J. Compos. Mater. **2**(3), 332–358 (1968). https://doi.org/10.1177/002199836800200305
28. Noor, A.K., Burton, W.S.: Computational models for high-temperature multilayered composite plates and shells. Appl. Mech. Rev. **45**(10), 419–446 (1992). https://doi.org/10.1115/1.3119742
29. Cook, R.D.: Concepts and applications of finite element analysis. Wiley, Hoboken (2007)
30. Sai Ram, K.S., Sinha, P.K.: Hygrothermal effects on the buckling of laminated composite plates. Compos. Struct. **21**(4), 233–247 (1992). https://doi.org/10.1016/0263-8223(92)90051-D
31. Reddy, J.N.: Mechanics of laminated composite plates and shells: theory and analysis. CRC Press, Boca Raton (2003)
32. Lal, R., Saini, R.: Buckling and vibration of non-homogeneous rectangular plates subjected to linearly varying in-plane force. J Shock Vib. **20**(5), 879–894 (2013). https://doi.org/10.3233/SAV-130791
33. Hamedani, S.J., Khedmati, M.R., Azkat, S.: Vibration analysis of stiffened plates using finite element method. Latin Am. J. Solids Struct. **9**(1), 1–20 (2012). https://doi.org/10.1590/S1679-78252012000100001
34. Patel, S., Sheikh, A.: Buckling response of laminated composite stiffened plates subjected to partial in-plane edge loading. Int. J. Comput. Methods Eng. Sci. Mech. **17**(5–6), 322–338 (2016). https://doi.org/10.1080/15502287.2016.1231235
35. Kalgutkar, A.P., Banerjee, S.: Dynamic instability analysis of perforated stiffened laminated composite panels subjected to non-uniform in-plane edge load under hygrothermal condition. Thin-Wall. Struct. **181**, 109961 (2022). https://doi.org/10.1016/j.tws.2022.109961
36. Dharmarajan, S., McCutchen, H.: Shear coefficients for orthotropic beams. J. Compos. Mater. **7**(4), 530–535 (1973). https://doi.org/10.1177/002199837300700411
37. Ugural, A.C., Fenster, S.K.: Advanced strength and applied elasticity. Prentice Hall, Hoboken (1995)
38. Bathe, K.-J.: Finite element procedures. Prentice Hall, Pearson Education, Inc (2006)
39. Sekine, H., Hu, N., Kouchakzadeh, M.A.: buckling analysis of elliptically delaminated composite laminates with consideration of partial closure of delamination. J. Compos. Mater. **34**(7), 551–574 (2000). https://doi.org/10.1177/002199830003400702
40. Parhi, P.K., Bhattacharyya, S.K., Sinha, P.K.: Hygrothermal effects on the dynamic behavior of multiple delaminated composite plates and shells. J. Sound Vib. **248**(2), 195–214 (2001). https://doi.org/10.1006/jsvi.2000.3506
41. Haynes, R.A.: Hygrothermally stable laminated composites with optimal coupling, School of Aerospace Engineering, Georgia Institute of Technology, Parkway, (2010)
42. Muder, S.: Hygrothermally stable laminated composites for optimal extension twist coupling in closed cell configuration. The University of Texas Arlington, Faculty of the Graduate School (2012)
43. Castro, S.G.P., Donadon, M.V.: Assembly of semi-analytical models to address linear buckling and vibration of stiffened composite panels with debonding defect. Compos. Struct. **160**, 232–247 (2017). https://doi.org/10.1016/j.compstruct.2016.10.026
44. Whitney, J.M., Ashton, J.E.: Effect of environment on the elastic response of layered composite plates. AIAA J. **9**(9), 1708–1713 (1971). https://doi.org/10.2514/3.49976